the FEBS Journal

Secondary structure of lipidated Ras bound to a lipid bilayer

Jörn Güldenhaupt[1,*], Yekbun Adigüzel[1,*], Jürgen Kuhlmann[2], Herbert Waldmann[2], Carsten Kötting[1] and Klaus Gerwert[1]

1 Lehrstuhl für Biophysik, Ruhr-Universität Bochum, Germany
2 Max Planck Institute of Molecular Physiology, Dortmund, Germany

Keywords
FTIR; GTPases; lipid anchor; membrane; proteins

Correspondence
K. Gerwert, Lehrstuhl für Biophysik, Ruhr-Universität Bochum, Universitätsstr. 150, D-44801 Bochum, Germany
Fax: +49 234 32 14238
Tel: +49 234 32 24461
E-mail: gerwert@bph.rub.de

*These authors contributed equally to this work

(Received 28 August 2008, revised 25 September 2008, accepted 1 October 2008)

doi:10.1111/j.1742-4658.2008.06720.x

Ras proteins are small guanine nucleotide binding proteins that regulate many cellular processes, including growth control. They undergo distinct post-translational lipid modifications that are required for appropriate targeting to membranes. This, in turn, is critical for Ras biological function. However, most *in vitro* studies have been conducted on nonlipidated truncated forms of Ras proteins. Here, for the first time, attenuated total reflectance-FTIR studies of lipid-modified membrane-bound N-Ras are performed, and compared with nonlipidated truncated Ras in solution. For these studies, lipidated N-Ras was prepared by linking a farnesylated and hexadecylated N-Ras lipopeptide to a truncated N-Ras protein (residues 1–181). It was then bound to a 1-palmitoyl-2-oleoyl-*sn*-glycero-3-phosphocholine bilayer tethered on an attenuated total reflectance crystal. The structurally sensitive amide I absorbance band in the IR was detected and analysed to determine the secondary structure of the protein. The NMR three-dimensional structure of truncated Ras was used to calibrate the contributions of the different secondary structural elements to the amide I absorbance band of truncated Ras. Using this novel approach, the correct decomposition was selected from several possible solutions. The same parameter set was then used for the membrane-bound lipidated Ras, and provided a reliable decomposition for the membrane-bound form in comparison with truncated Ras. This comparison indicates that the secondary structure of membrane-bound Ras is similar to that determined for the nonlipidated truncated Ras protein for the highly conserved G-domain. This result validates the multitude of investigations of truncated Ras without anchor *in vitro*. The novel attenuated total reflectance approach opens the way for detailed studies of the interaction network of the membrane-bound Ras protein.

Ras proteins are molecular switches [1] that operate in distinct cellular activities as mediators in cell signalling cascades from receptor tyrosine kinases to the nucleus, through the activation of downstream effectors, to stimulate, for example, growth and differentiation [2,3]. During its activity, Ras is bound to the inner leaflet of the cellular membrane with its C-terminus [4]. The C-terminus is hypervariable and this, in turn, results in different Ras isoforms (H-, N- and K-Ras), which are recruited to different membrane platforms. All isoforms are otherwise very similar in structure and function. They terminate in a CAAX (C, Cys; A, aliphatic; X, variety of amino acids) motif initially, which undergoes sequential farnesylation at Cys186,

Abbreviations
ATR, attenuated total reflectance; FWHH, full width at half-height; GFP, green fluorescent protein; IRE, internal reflection element; POPC, 1-palmitoyl-2-oleoyl-*sn*-glycero-3-phosphocholine.

AAX proteolysis and methylesterification. H-Ras is then palmitoylated at Cys181 and Cys184, whereas N-Ras is palmitoylated at Cys181 only. K-Ras has a polybasic domain instead, which spans residues 175–180 [5].

In vitro studies on lipidated Ras have included the NMR characterization of farnesylated versus nonfarnesylated H-Ras in solution, but not membrane bound [6], NMR studies on the dynamics of the lipid anchor in the membrane [7,8], studies of membrane binding by surface plasmon resonance [9] and grazing incidence X-ray diffraction [10], molecular dynamics simulations [11] and orientation of membrane-bound Ras by internal reflection IR spectroscopy [12]. Two lipid anchors are necessary for stable membrane insertion [9]. Membrane localization has been investigated using fluorescence labels and atomic force microscopy [13]. Either green fluorescent protein (GFP)–Ras constructs [14] or chemically modified anchors [15] have been used. It has been shown that lipid modification governs membrane localization. After *S*-palmitoylation of H-Ras and N-Ras at the Golgi, vesicular transport towards the plasma membrane follows. The subsequent hydrolysis of the ester closes this cycle [14]. Acyl protein thioesterase 1 is probably important for this process [16]. In addition to localization, lipid anchors may also be involved directly in protein–protein interactions with guanine nucleotide exchange factors [17] and effectors [18].

We used double lipid-anchored N-Ras protein possessing one farnesyl and one hexadecyl lipid moiety [9]. The Ras lipopeptide was attached to the C-terminus with a maleimidocaproyl group (Fig. 1). The natural palmitoyl moiety was replaced by the nonhydrolysable hexadecyl moiety during our measurements. Binding of this protein to solid supported 1-palmitoyl-2-oleoyl-*sn*-glycero-3-phosphocholine (POPC) model membranes was investigated using attenuated total reflectance (ATR)-FTIR spectroscopy. For comparison, C-terminally truncated Ras (H-Ras 1–166) without lipid modification was used. This form has been used in most *in vitro* investigations so far. We present a novel approach for the decomposition of the amide I band into its secondary structural elements [19]. First, we calibrated the parameter set of the decomposition with an X-ray or NMR structural model. Using this parameter set, only the peak heights of the absorptions of the secondary structural elements need to be optimized in further decompositions. By doing this, the intrinsic underestimation of the decomposition is largely reduced and clear-cut for the relative changes. Here, the structural differences between the secondary structure of Ras in solution and membrane bound were determined within an accuracy of 3%, because the same parameter set was used.

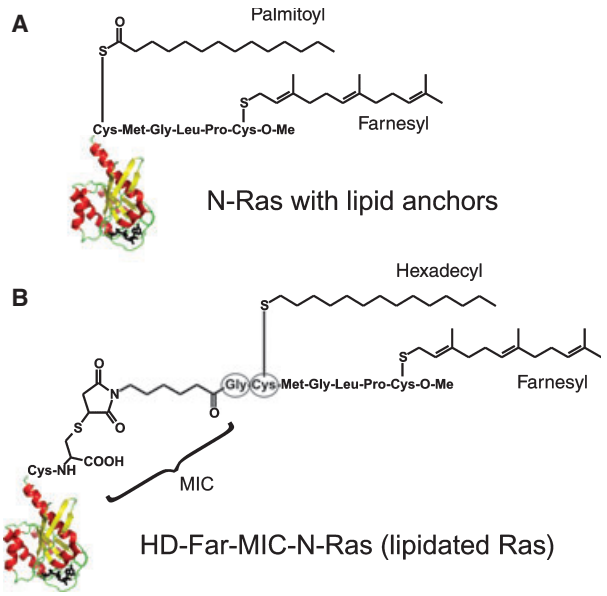

Fig. 1. (A) Natural N-Ras protein with the lipid anchors at residues 181 and 186. (B) For the lipidated Ras in this investigation, we used a peptide attached to Cys181 of N-Ras via a maleimidocaproyl group and the anchors attached to residues 183 and 188, leading to two additional residues (encircled).

Results

Lipid bilayer formation and protein adsorption

For the measurements of membrane-bound lipidated Ras, the lipid layer was first formed on the ATR surface. Lipid self-assembly was directly monitored by the time-dependent absorbance increase in its methylene stretching vibrations (Fig. 2A).

The buffer spectrum was subtracted as the reference. The stability of the evolved bilayer was attained in 10–15 min (Fig. 2B). The time-dependent absorption was the same as observed previously with a quartz crystal microbalance by Richter *et al.* [20], who showed by atomic force microscopy (AFM) that a single bilayer was formed. Thus, we are confident that we have a single bilayer of a similar quality. We checked the completeness of our layer using BSA. The latter strongly adsorbs at germanium, giving a strong amide I absorbance. The same experiment with the POPC layer gave an increase of less than 1% compared with the latter experiment. Thus, it was concluded that the POPC layer was at least 99% complete. Further, the lipid layer durability was assured by monitoring the absorbance of the lipid during the experiment. Specific

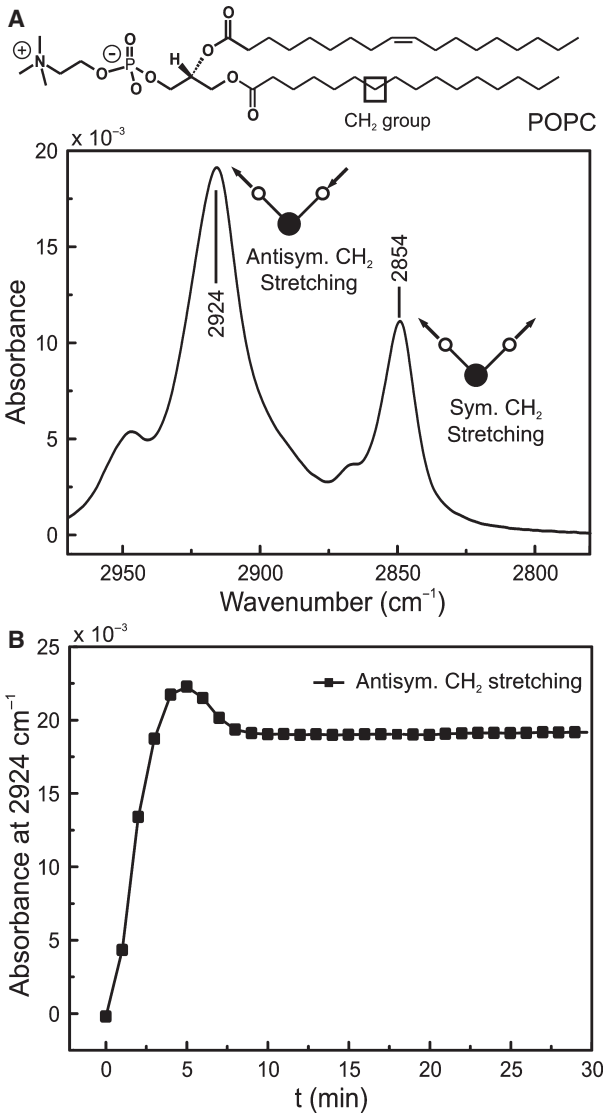

Fig. 2. (A) ATR-FTIR absorbance of POPC methylene stretching vibrations. (B) Model membrane adsorption kinetics on the IRE surface observed at 2924 cm^{-1}.

binding of the double lipid-anchored N-Ras protein on solid supported POPC model membranes was attained and the IR spectra were measured. Truncated Ras was used as a control and showed no binding.

In Fig. 3, the absorbance increase in the amide I band with time is shown for the membrane-anchored and truncated Ras. The membrane-bound N-Ras protein was fully active within our set-up, as shown by an activity test based on the ability to catalyse GTP hydrolysis. For this purpose, the change in time of the GDP/GTP ratio was determined by HPLC. The lipid to protein ratio was calculated as described above, and found to be about 150 ± 30 lipid molecules per

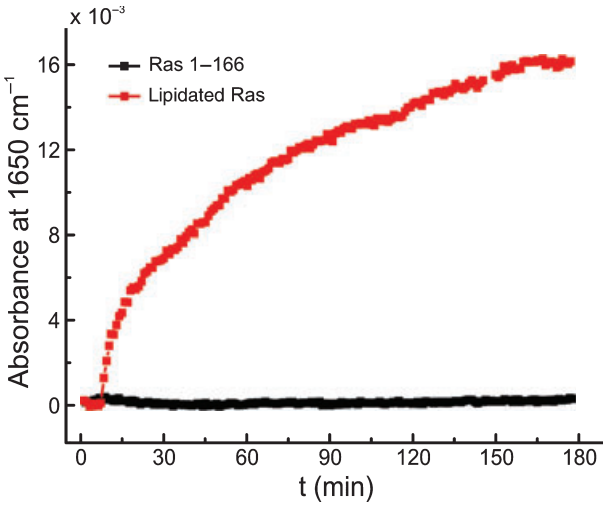

Fig. 3. Protein adsorption kinetics of lipidated Ras and truncated Ras on the POPC model membrane observed by the amide I absorbance at 1650 cm^{-1}.

lipidated Ras protein. This corresponds to a monolayer with relatively densely packed Ras.

Curve-fitting analysis

The original absorbance spectrum in the amide I′ and II regions with the side-chain contribution is shown in Fig. 4. The side-chain contribution was subtracted until the tyrosine side-chain absorbance at 1515 cm^{-1} disappeared. Side-chain absorbances were removed from the amide I′ region because they overlap with the amide I′ absorption.

Our parameter set was calibrated by decomposition of the truncated wild-type H-Ras transmission

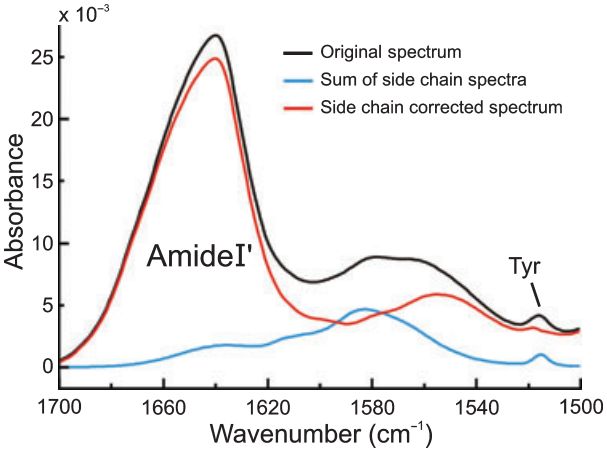

Fig. 4. Amide I′ and II regions of the original spectrum (black), its side-chain spectrum (blue) and the side-chain-corrected spectrum (red). A transmission measurement of truncated Ras is shown.

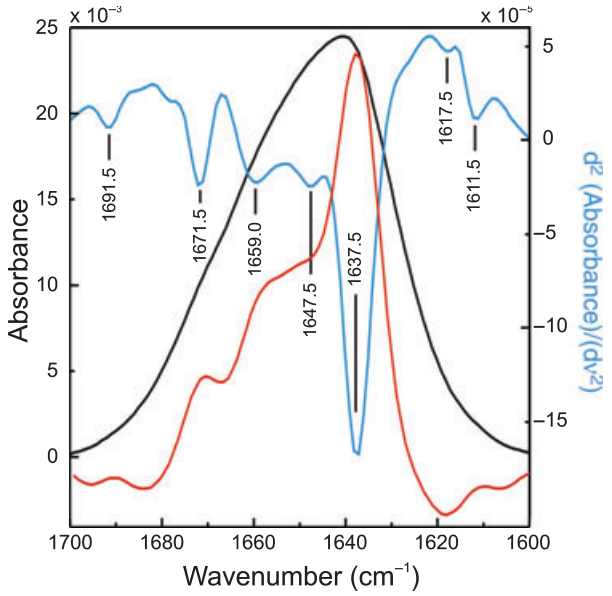

Fig. 5. The side-chain-corrected amide I′ absorbance of a transmission measurement of truncated Ras (black) and its second derivative (blue) and its Fourier self-deconvolution [red, with FWHH = 30 cm^{-1} (Gaussian) and 13.6 cm^{-1} (Lorentzian)]. The latter was scaled by a factor of 0.4. The minima of the second derivative and the maxima of the Fourier self-deconvolution were used as starting positions for the fitting procedure.

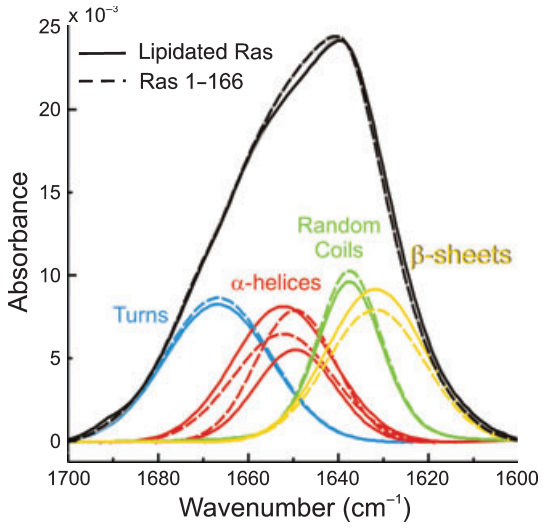

Fig. 6. The amide I′ regions of an ATR-FTIR measurement of membrane-bound lipidated Ras and a transmission measurement of truncated Ras are shown in comparison with their underlying backbone absorbance of the secondary structural elements. Secondary structure volume differences are indicated with the same colour as their respective spectra. The spectra were normalized to give an area of unity for the amide I band.

spectrum with the corresponding NMR structure in solution (pdb 1CRP [21]). The number and positions of the individual secondary structural elements underlying the amide I′ curve can be estimated using the local minima of its second derivative and the local maxima of its Fourier self-deconvolution (Fig. 5). First, a decomposition with four components was attempted, but the fit was not in agreement with the NMR structural model (rmsd = 9.2 %). However, a fit using five components yielded a standard deviation from the measured spectrum of 6.25×10^{-6} and rmsd between IR and NMR of 1.1%. The bands obtained were assigned to the respective secondary structures that they represented: 1666.6 cm^{-1} (turn), 1652.1 cm^{-1} (α-helix), 1649.4 cm^{-1} (α-helix), 1637.4 cm^{-1} (random coil) and 1631.6 cm^{-1} (β-sheet). This parameter set with fixed band positions, full widths at half-height (FWHHs) and Gaussian/Lorentzian fractions was used to decompose the membrane-bound form by optimizing only the peak heights for each component, as described previously [19]. Therefore, the error of the secondary structure change is much lower than the error of the absolute secondary structure determination.

The decomposition of truncated Ras in solution and of membrane-bound Ras is shown in Fig. 6. It was assumed for the decomposition that the extinction coefficients were equal for all of the secondary structural elements of the protein. The two very similar amide I′ bands showed no unusual broadening, which would point to protein denaturation. The results of the secondary structural analyses are summarized in Table 1. Much larger changes are observed, for example, in the prion protein folding from α-helix to β-sheet [22].

For our calibration, we favoured the NMR (pdb 1CRP [21], column 3) over the X-ray (pdb 4Q21 [23], column 2) structural model, because it was also measured in solution. Furthermore, it resembles the mean of an ensemble of 20 structures and thus indicates the dynamics of the protein, leading to changes in secondary structure according to the stride algorithm by 3%. It should be noted that the X-ray structure deviates by up to 6% from the NMR structure. In particular, the random coil content of the NMR structure increases by 10 amino acids as compared to the X-ray structure. In our calibration, good agreement of the decomposition of our transmission FTIR measurement (column 4, rmsd less than 3%) with the NMR data (pdb 1CRP) was obtained. It is also possible to calibrate the decomposition by means of the X-ray structure, leading to another parameter set. However, the overall fit is slightly better for the NMR structure-based calibration set.

Table 1. X-Ray and NMR-based secondary structure of Ras in comparison with the protein spectra curve-fitting results of this work (columns 5 and 6) (aa, amino acid).

	Truncated Ras 1–166 from X-ray (4Q21 cut to 1–166)	Truncated Ras 1–166 from NMR (1CRP, average of 20 models)	Truncated Ras 1–166 (average of four measurements)	Membrane-bound lipidated Ras 1–188 (average of three measurements)	Estimated structure of the anchor region 167–188
β-sheets	25.9% = 43 aa	22.3 ± 1.9% = 37 ± 3 aa	21.0 ± 3% = 35 ± 5 aa	25.1 ± 3% = 47 ± 6 aa	12
Random coils	13.3% = 22 aa	19.4 ± 2.6% = 32 ± 4 aa	20.0 ± 3% = 33 ± 5 aa	18.1 ± 3% = 34 ± 6 aa	1
α-helices	37.3% = 62 aa	35.5 ± 1.1% = 59 ± 2 aa	34.5 ± 3% = 57 ± 5 aa	33.3 ± 3% = 63 ± 6 aa	6
Turns	23.5% = 39 aa	22.8 ± 2.5% = 38 ± 4 aa	24.6 ± 3% = 41 ± 5 aa	23.5 ± 3% = 44 ± 6 aa	3
Standard deviation			6.25×10^{-6}	1.45×10^{-5}	

The secondary structure analysis of membrane-bound lipidated Ras using the same parameter set, optimizing only the five peak heights, is shown in column 5. Here, we have taken into account the additional residues 167–188. Thus. it is easier to compare the corresponding number of amino acids, instead of the percentages of secondary structure. Overall, the secondary structures of truncated and lipidated Ras are in very good agreement. Because the same parameter set was used for all decompositions, possible structural changes are reliably determined.

In principle, secondary structure analysis using an ATR set-up contains a systematic error if the sample is oriented, as the electric fields for vertical and perpendicular polarized light are different [24]. However, Ras is less oriented compared with transmembrane proteins or even surface-adsorbed small organic molecules. In order to probe this effect, we performed polarized measurements and used the correction recommended by Marsh [24]. This led to no significant deviations (< 1%) from our analysis. Therefore, we neglected this effect.

Discussion

As shown in Fig. 6 and Table 1, the secondary structures of truncated Ras and full-length membrane-bound Ras are very similar. Therefore, it seems reasonable to assume that the G-domain is conserved. If we assume that there is no change within the G-domain, we can estimate the secondary structure of the additional residues 167–188, as shown in column 6 of Table 1. We have an increase in α-helical content of about six residues. This agrees with an NMR investigation [6,7], which showed an extension of the C-terminal α-helix to residue 172. Although only a very small random coil increase was observed, a significant β-sheet content of the anchor region was detected. Interestingly, an NMR investigation of the C-terminal heptapeptide [7] (D. Huster, Universität Leipzig, Germany; personal communication) also showed, despite the extensive dynamics of this region, mainly β-sheet structure.

As summarized in Fig. 7, truncated Ras and membrane-anchored full-length Ras show the same secondary structure within the accuracy of our method. Meister *et al.* [12] investigated lipidated Ras binding to a lipid layer using IR reflection-absorption spectroscopy. In this study, it was assumed that the secondary structure remains unaltered, and the observed changes in the spectra were assigned to different orientations. An advantage of the IR reflection-absorption spectroscopy set-up is that the air–water interface is always flat. Therefore, changes in the orientation can be reliably determined. However, this is possible only at the expense of the signal-to-noise ratio, and the signal of membrane-anchored Ras was outside the detection limit. Instead, the structure of Ras at the air–water interface was analysed. With the largely increased signal-to-noise ratio of ATR-FTIR, we have, for the

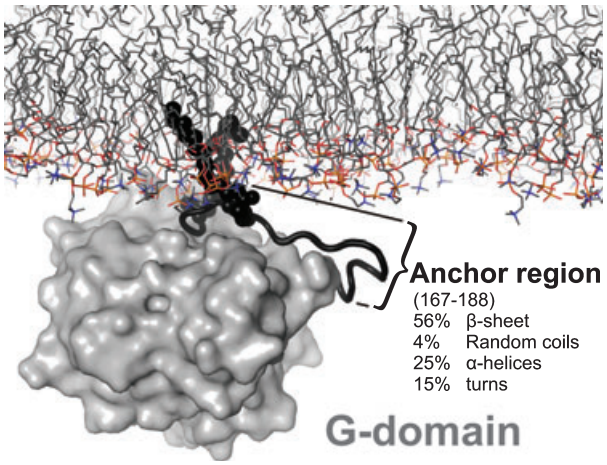

Fig. 7. Secondary structure of the anchor region of membrane-bound N-Ras according to our results, assuming a structurally unchanged G-domain. The three-dimensional model was built according to NMR structures [6,8,21].

first time, obtained a high-quality IR spectrum of Ras bound by its lipid anchors to a membrane. We found that the secondary structure is not affected by membrane binding when compared with the NMR structure of truncated Ras. Thus, the assumption of Meister *et al*. [12], to assign the observed changes to the orientation changes of the Ras protein, is confirmed. Interestingly, molecular dynamics simulations of membrane-bound Ras protein gave similar results [11]. Two modes of binding were found, which again differ mainly in orientation but not in secondary structure. Recently, combined fluorescence resonance energy transfer measurements on live cells and molecular dynamics simulations of membrane-bound Ras protein have suggested that the β2–β3-loop and the α5-helix act as a novel switch by conformational changes [25].

Conclusions

For the first time, the secondary structure of the N-Ras protein bound with two anchors to a lipid bilayer has been determined and compared with the secondary structures of truncated Ras, from which the X-ray and NMR structures were determined. Both agree well within experimental error. Thus, our results validate the numerous *in vitro* investigations of truncated Ras carried out previously. Further, we propose that the secondary structure of the anchor region is mainly α-helix and β-sheet.

This study establishes FTIR spectroscopy of membrane-bound Ras protein as a new tool, paving the way to revealing the dynamic interactions of membrane-bound N-Ras protein with its effectors and regulators (i.e. Ras binding domain of Raf, guanine nucleotide exchange factors and GTPase activating proteins), including possible influences of Ras orientation. Such studies can be used to study the influence of small molecules for molecular therapy on the Ras interaction network.

Experimental procedures

Materials

POPC was purchased from Lipoid (Lipoid GmbH, Ludwigshafen, Germany). Lipid solutions at a concentration of about 32 mM were prepared using chloroform. Lipid vesicle solutions were prepared in D_2O (Deutero GmbH, Kastellaun, Germany) buffer (20 mM Tris/HCl, pD 7.4, 5 mM $MgCl_2$, 2 mM dithioerythritol). A 40.8 $g{\cdot}L^{-1}$ protein stock solution was used for the injection of N-Ras protein onto the buffer solution of the adsorbed POPC model membrane. All experiments were carried out in the same deuterated buffer medium as given above at room temperature. The absence of H_2O was checked in the O–H stretching region of the spectrum.

A vertical ATR multireflection unit (Specac, Orpington, UK) mounted in an IFS66 spectrometer (BrukerOptics, Ettlingen, Germany) was used for the measurements. The internal reflection element (IRE) was a $52 \times 20 \times 2$ mm trapezoidal germanium ATR plate with an aperture angle of 45° yielding 25 internal reflections.

The expression and purification of truncated H-Ras have been described elsewhere [26]. For the synthesis of the farnesylated and hexadecylated N-Ras lipopeptide, truncated (residues 1–181) wild-type N-Ras was expressed in *Escherichia coli* CK600K strain, and then purified using DEAE ion exchange chromatography and gel filtration. Chemically synthesized N-Ras lipopeptide [27–29] was coupled to the protein in 20 mM Tris/HCl, pH 7.4, 5 mM $MgCl_2$, saturated with the detergent Triton X 114. The detergent was removed by DEAE ion exchange chromatography and the lipoprotein was concentrated in 20 mM Tris/HCl, pH 7.4, 5 mM $MgCl_2$, 2 mM dithioerythritol by size exclusion filtration, using Amicon® concentrators. All protein batches were analysed by SDS-PAGE and MALDI-TOF-MS.

Preparation of the ATR crystal

The germanium IRE of the ATR was cleaned chemically with a mixture of chloroform and methanol, followed by rinsing; the hydrophilic character of the crystal surface was obtained by dipping it in sulfuric acid solution. The crystal was rinsed again with double-distilled water and the surface was dried under a nitrogen flow. Finally, an organic solvent was applied to remove the lipid remnants. The temperature was set to 292 K for all experiments.

Bilayer formation

POPC (12.9 μL) in chloroform was taken from a 25 $mg{\cdot}mL^{-1}$ stock solution in an Eppendorf tube, and two volumes of chloroform were added for POPC small unilamellar vesicle preparation. Chloroform was then evaporated under a mild nitrogen flow and subsequently kept under vacuum for 2 h for complete removal of the chloroform remnants. Deuterated buffer solution (50 μL) was added to the multilayered dry lipid film and incubated for 1 h at room temperature with shaking in a Thermomixer (Eppendorf, Hamburg, Germany) at 1200 min^{-1}. The resulting solution after this treatment was a multilamellar vesicle solution. A small unilamellar vesicle solution was prepared from the multilamellar vesicle solution by sonification in an ice-cold water bath for 7 min. Clearance of the opaque lipid solution indicated the formation of vesicles with a radius of less than 100 nm, and was checked by measurement with a

High-Performance Particle Sizer using NIBS™ Technology from Malvern Instruments (Malvern, Worcestershire, UK).

POPC small unilamellar vesicles (~ 0.3 mM, 1.2 mL) were brought into contact with the clean hydrophilic surface of the solid support to initiate the vesicle fusion process on IRE [20]. Spectral collection was started immediately after sample application. The incubation period for lipid layer assembly was 30 min. The system was then flushed with 10 mL of deuterated buffer through the sampling system using a peristaltic pump-induced flow.

Protein incorporation

After the formation of the model membrane, protein incorporation was initiated by mixing the protein into the sample solution on the surface. The starting bulk concentration of the protein was approximately 2.0 μM in a buffer containing 20 mM Tris/Cl, 5 mM $MgCl_2$, 1 mM dithiothreitol and 0.1 mM GDP at pD 7.8. Protein adsorption on to the membrane was followed by the evolution of the amide I and II (amide I′ and II′ in the case of deuterated buffer) bands. The measurements were performed with the protein in deuterated buffer. Measurements were carried out at room temperature and performed at an instrument resolution of 2 cm^{-1} with four times zero filling. Three-term Blackman–Harris apodization was applied and 600 scans were averaged for each spectrum.

Lipid to protein ratio

The lipid to protein ratio was estimated from the ratio of the areas of the lipid (C=O) absorption at around 1750 cm^{-1} and the side-chain absorbance-corrected protein amide I′ absorption. This ratio was divided by the ratio of the respective number of carbonyl groups per molecule (two for POPC and 188 for lipidated Ras). This result is a rough estimate, neglecting differences in extinction coefficients and evanescent wave decay.

Curve-fitting analysis

First, all spectra were corrected for water vapour contribution manually and smoothed by apodization with a Gaussian band shape with 4 cm^{-1} FWHH. Then, the contribution of the side-chains to the protein spectrum was computed within the amide I′ and II′ regions. This was performed using the kinetics software (provided by E. Goormaghtigh) running under MATLAB (version R12, Mathworks, Natick, MA, USA). The contributions of the side-chains were then rebuilt according to the data given in the literature [30], and were scaled and subtracted to eliminate the tyrosine ring vibration band at 1515 cm^{-1}. In addition, a linear baseline correction between 1600 and 1700 cm^{-1} was performed. Before curve fitting, the second derivatives of the smoothed spectra were inspected in order to estimate the number and positions of the bands needed to deconvolute the amide I′ absorption. Least-squares iterative curve fitting was performed to fit a mixture of Lorentzian and Gaussian line shapes to the spectrum between 1700 and 1600 cm^{-1}, as initially described by Goormaghtigh *et al.* [31] and improved by Ollesch *et al.* [19]. The decomposition of the amide I band does not provide an unequivocal result, because the analysis is, in principle, as in CD spectroscopy, experimentally underdetermined. However, a novel approach was introduced in which the decomposition of the truncated form of Ras is calibrated by an NMR structure (pdb 1CRP [21]). This selects from several possible decompositions that which agrees with the secondary structure as determined by NMR in solution. The obtained parameter set (number of bands and positions, FWHHs and Gaussian/Lorentzian fractions for each band) was then used to decompose the amide I band of membrane-bound Ras, where only the peak heights were fitted. They reflect the contributions of the secondary structure elements. Our novel approach provides a reliable analysis, especially of the changes in secondary structure, and is described in detail in Ollesch *et al.* [19]. Each experimental set was repeated three times and the curve-fitting analyses were performed with randomly selected spectra from each set. The results showed less than 3% deviation. This value is the approximate error. It was the same as that reported previously [19] for this method.

The quality of curve fitting was evaluated through the standard deviation of the fit, as the mean displacement of the curve-fitted resultant spectrum from the original. The rmsd values for the secondary structure content were calculated according to the formula:

$$\mathrm{rmsd} = \sqrt{\frac{1}{N}\sum_{i=1}^{i=N}\delta_i^2}, \qquad (1)$$

where N is the total number of components, namely the number of secondary structural elements, and δ_i is the deviation of the structural component from its reported value in the literature.

ATR measurements

We have presented in this study the sample preparation of membrane-bound lipidated N-Ras protein on solid supported POPC model membranes as a tool for membrane protein interaction studies performed with the ATR-FTIR technique [32]. The refractive index of germanium IRE is 4.0 at 1000 cm^{-1} and the penetration depth of the evanescent wave at 1650 cm^{-1} is approximately 1.5 μm. It should be noted that the usual linear ATR correction for the wavelength dependence of the penetration depth is not necessary, because our sample is only a monolayer close to IRE. Within a 10 nm layer, the

intensity of the electric field changes by only 0.1% between 1600 and 1700 cm^{-1}.

Acknowledgements

The authors wish to acknowledge the Max Planck Institute of Molecular Physiology in Dortmund and SFB 642 for financial support. We thank Angela Kallenbach for providing H-Ras (1–166) and Till Rudack for help with Fig. 7.

References

1 Vetter IR & Wittinghofer A (2001) Signal transduction – the guanine nucleotide-binding switch in three dimensions. *Science* **294**, 1299–1304.
2 Downward J (2003) Targeting RAS signalling pathways in cancer therapy. *Nat Rev Cancer* **3**, 11–22.
3 Malumbres M & Barbacid M (2003) Timeline – RAS oncogenes: the first 30 years. *Nat Rev Cancer* **3**, 459–465.
4 Willumsen BM, Christensen A, Hubbert NL, Papageorge AG & Lowy DR (1984) The P21 Ras C-terminus is required for transformation and membrane association. *Nature* **310**, 583–586.
5 Wittinghofer A & Waldmann H (2000) Ras – a molecular switch involved in tumor formation. *Angew Chem Int Edit* **39**, 4192–4214.
6 Thapar R, Williams JG & Campbell SL (2004) NMR characterization of full-length farnesylated and non-farnesylated H-ras and its implications for raf activation. *J Mol Biol* **343**, 1391–1408.
7 Reuther G, Tan KT, Kohler J, Nowak C, Pampel A, Arnold K, Kuhlmann J, Waldmann H & Huster D (2006) Structural model of the membrane-bound C terminus of lipid-modified human N-ras protein. *Angew Chem Int Edit* **45**, 5387–5390.
8 Reuther G, Tan KT, Vogel A, Nowak C, Arnold K, Kuhlmann J, Waldmann H & Huster D (2006) The lipidated membrane anchor of full length N-Ras protein shows an extensive dynamics as revealed by solid-state NMR spectroscopy. *J Am Chem Soc* **128**, 13840–13846.
9 Bader B, Kuhn K, Owen DJ, Waldmann H, Wittinghofer A & Kuhlmann J (2000) Bioorganic synthesis of lipid-modified proteins for the study of signal transduction. *Nature (London)* **403**, 223–226.
10 Bringezu F, Majerowicz M, Wen SY, Reuther G, Tan KT, Kuhlmann J, Waldmann H & Huster D (2007) Membrane binding of a lipidated N-Ras protein studied in lipid monolayers. *Eur Biophys J Biophys* **36**, 491–498.
11 Gorfe AA, Hanzal-Bayer M, Abankwa D, Hancock JF & McCammon JA (2007) Structure and dynamics of the full-length lipid-modified H-ras protein in a 1,2-dimyristoylglycero-3-phosphocholine bilayer. *J Med Chem* **50**, 674–684.
12 Meister A, Nicolini C, Waldmann H, Kuhlmann J, Kerth A, Winter R & Blume A (2006) Insertion of lipidated Ras proteins into lipid monolayers studied by infrared reflection absorption spectroscopy (IRRAS). *Biophys J* **91**, 1388–1401.
13 Nicolini C, Baranski J, Schlummer S, Palomo J, Lumbierres-Burgues M, Kahms M, Kuhlmann J, Sanchez S, Gratton E, Waldmann H *et al.* (2006) Visualizing association of N-Ras in lipid microdomains: influence of domain structure and interfacial adsorption. *J Am Chem Soc* **128**, 192–201.
14 Rocks O, Peyker A, Kahms M, Verveer PJ, Koerner C, Lumbierres M, Kuhlmann J, Waldmann H, Wittinghofer A & Bastiaens PIH (2005) An acylation cycle regulates localization and activity of palmitoylated Ras isoforms. *Science* **307**, 1746–1752.
15 Reents R, Wagner M, Kuhlmann J & Waldmann H (2004) Synthesis and application of fluorescence-labeled Ras-proteins for live-cell imaging. *Angew Chem Int Edit* **43**, 2711–2714.
16 Deck P, Pendzialek D, Biel M, Wagner M, Popkirova B, Ludolph B, Kragol G, Kuhlmann J, Giannis A & Waldmann H (2005) Development and biological evaluation of acyl protein thioesterase 1 (APT1) inhibitors. *Angew Chem Int Edit* **44**, 4975–4980.
17 Porfiri E, Evans T, Chardin P & Hancock JF (1994) Prenylation of Ras proteins is required for efficient Hsos1-promoted guanine-nucleotide exchange. *J Biol Chem* **269**, 22672–22677.
18 Rubiol I, Wittig U, Meyer C, Heinze R, Kadereit D, Waldmann H, Downward L & Wetzker R (1999) Farnesylation of Ras is important for the interaction with phosphoinositide 3-kinase gamma. *Eur J Biochem* **266**, 70–82.
19 Ollesch J, Kunnemann E, Glockshuber R & Gerwert K (2007) Prion protein alpha-to-beta transition monitored by time-resolved Fourier transform infrared spectroscopy. *Appl Spectrosc* **61**, 1025–1031.
20 Richter R, Mukhopadhyay A & Brisson A (2003) Pathways of lipid vesicle deposition on solid surfaces: a combined QCM-D and AFM study. *Biophys J* **85**, 3035–3047.
21 Kraulis PJ, Domaille PJ, Campbell-Burk SL, Van Aken T & Laue ED (1994) Solution structure and dynamics of Ras p21.GDP determined by heteronuclear three- and four-dimensional NMR spectroscopy. *Biochemistry* **33**, 3515–3531.
22 Elfrink K, Ollesch J, Stöhr C, Willbold D, Riesner D & Gerwert K (2008) Structural changes of membrane anchored PrPC. *Proc Natl Acad Sci USA* **105**, 10815–10819.

23 Milburn MV, Tong L, Devos AM, Brunger A, Yamaizumi Z, Nishimura S & Kim SH (1990) Molecular switch for signal transduction – structural differences between active and inactive forms of protooncogenic Ras proteins. *Science* **247**, 939–945.
24 Marsh D (1999) Quantitation of secondary structure in ATR infrared spectroscopy. *Biophys J* **77**, 2630–2637.
25 Abankwa D, Hanzal-Bayer M, Ariotti N, Plowman SJ, Gorfe AA, Parton RG, McCammon JA & Hancock JF (2008) A novel switch region regulates H-ras membrane orientation and signal output. *EMBO J* **27**, 727–735.
26 Tucker J, Sczakiel G, Feuerstein J, John J, Goody RS & Wittinghofer A (1986) Expression of p21 proteins in *Escherichia coli* and stereochemistry of the nucleotide-binding site. *EMBO J* **5**, 1351–1358.
27 Kuhn K, Owen DJ, Bader B, Wittinghofer A, Kuhlmann J & Waldmann H (2001) Synthesis of functional Ras lipoproteins and fluorescent derivatives. *J Am Chem Soc* **123**, 1023–1035.
28 Nagele E, Schelhaas M, Kuder N & Waldmann H (1998) Chemoenzymatic synthesis of N-Ras lipopeptides. *J Am Chem Soc* **120**, 6889–6902.
29 Schelhaas M, Glomsda S, Hansler M, Jakubke HD & Waldmann H (1996) Enzymatic synthesis of peptides and Ras lipopeptides employing choline ester as a solubilizing, protecting, and activating group. *Angewandte Chemie-Int Edn Eng* **35**, 106–109.
30 Barth A & Zscherp C (2002) What vibrations tell about proteins. *Q Rev Biophys* **35**, 369–430.
31 Goormaghtigh E, Cabiaux V & Ruysschaert J-M (1994) Determination of soluble and membrane protein structure by Fourier transform infrared spectroscopy. I. Assignments and model compounds. *Subcell Biochem* **23**, 329–362.
32 Wenzl P, Fringeli M, Goette J & Fringeli UP (1994) Supported phospholipid-bilayers prepared by the Lb/vesicle method – a Fourier-transform infrared attenuated total-reflection spectroscopic study on structure and stability. *Langmuir* **10**, 4253–4264.